Cellulose
DOI 10.1007/s10570-016-1030-y

ORIGINAL PAPER

Copper nanoparticles-sputtered bacterial cellulose nanocomposites displaying enhanced electromagnetic shielding, thermal, conduction, and mechanical properties

Pengfei Lv · Anfang Wei · Yiwen Wang · Dawei Li · Jin Zhang · Lucian A. Lucia · Qufu Wei

Received: 15 May 2016 / Accepted: 30 July 2016

Abstract Nanoscale bacterial cellulose (BC) may be functionalized to provide advanced eco-friendly substrates. In the current work, BC was functionalized by magnetron sputtering of copper (Cu) to endow it with unique electromagnetic shielding properties while concomitantly improving mechanical, thermal, and conduction properties. The surface morphologies and chemical characteristics of BC/Cu nanocomposites were studied by atomic force microscope, Fourier transform infrared spectroscopy, thermogravimetric analysis, X-ray diffraction and energy dispersive X-ray analysis system to conclusively demonstrate that Cu nanoparticles were evenly deposited on the surfaces. This topological construct enhanced the thermal stability, surface conductivity, mechanical properties, and interference (EMI) shielding effectiveness. EMI effects were also investigated by the four-point probe, uniaxial testing machine and a vector network analyzer that showed the BC/Cu nanoscale materials have high conductivity (0.026 S m^{-1}), good mechanical properties (41.4 Mpa) and excellent EMI shielding (55 dB).

Keywords Bacterial cellulose · Copper · Magnetron sputtering · Conductivity · Mechanical strength · Electromagnetic interference shielding · Thermal properties

Introduction

Recently, increasing attention has been paid to the development of microwave absorbing and insulation materials for electromagnetic interference (EMI) shielding (Che et al. 2004; Lakshmi et al. 2009; Song

A1 P. Lv · Y. Wang · D. Li · J. Zhang · Q. Wei (✉)
A2 Key Laboratory of Eco-Textiles, Jiangnan University,
A3 Wuxi 214122, China
A4 e-mail: qfwei@jiangnan.edu.cn

A5 P. Lv
A6 e-mail: 6130703014@vip.jiangnan.edu.cn

A7 Y. Wang
A8 e-mail: zhanghanhan2000@sina.com

A9 D. Li
A10 e-mail: ldw19900323@163.com

A11 J. Zhang
A12 e-mail: 6140708013@vip.jiangnan.edu.cn

A13 A. Wei
A14 Key Laboratory of Textile Fabric, Anhui Polytechnic
A15 University, Wuhu 241000, Anhui, China
A16 e-mail: wanfang2564@yahoo.com.cn

A17 L. A. Lucia (✉)
A18 Fiber and Polymer Science Program, North Carolina State
A19 University, 2401 Research Drive,
A20 Campus Box 8301, Raleigh, NC 27695-8301, USA
A21 e-mail: lalucia@ncsu.edu

Published online: 16 August 2016

et al. 2009; Yang et al. 2005b) within the context of human safety and sustainable development initiatives (Cao et al. 2010). EMI shielding effectiveness (SE), defined by the parameter decibel (dB), is important in the development of electronic materials in which 30 dB of SE is satisfactory when the attenuation of EMI radiation is 99.9 % (Huang 2003; Markham 1999; Yang et al. 2005a). Microwave absorbers, which can assimilate such radiation, are required for many low-cost, broadband and flexible industrial applications.

Copper (Cu) has been used as a conductive material for many years, because it possesses lower resistance than Al and lower cost than Ag (Tyagi et al. 2000). Cu nanowires, in fact, have found a niche following intensive studies in electroplating (Edelstein et al. 1997). Bacterial cellulose (BC) as synthesized by *Acetobacter xylinum* has a three dimensional web structure with nanofibril diameters (30–70 nm) (Chen et al. 2013) and displays fascinating features including high ultrafine porosity, high crystallinity, water absorbance, high tensile, biocompatibility, ease of chemical modification, cost (Klemm et al. 2001), and moldability during formation relative to natural cellulose (Sen et al. 2008). It has thus become a very useful biomaterial for many practical applications including reinforcing materials, supercapacitance, artificial blood vessels, electrochemical device (Jonas and Farah 1998; Petersen and Gatenholm 2011), stretchable conductors, highly conductive materials (Liang et al. 2012), lithium ion battery anodes (Wang et al. 2013a), and conductive and fire-resistant aerogels (Wang et al. 2013b). Furthermore, BC has become an attractive substrate for porous aerogel nanocomposites that exhibit unique mechanical and physical properties, including novel membrane materials (PengFei et al. 2016; Wen et al. 2013; Zheng et al. 2014).

BC by virtue of its physical and chemical versatility can be endowed with conductivity with conductivity within polymer composites (CPCs). Nowadays, several BC based electromagnetic shielding materials have been reported, e.g. polypyrrole/BC (15 dB) (Lian et al. 2015), $CoFe_2O_4$/BC (25 dB) (Han et al. 2015). Similarly, BC with filler in composites were also investigated to improve EMI SE, such as Fe_3O_4/BC (Marins et al. 2013) and $FeCl_3$/PAni BC (Marins et al. 2014). Within electronics, a device is termed electromagnetically compatible if it is not affected by fields arising from other devices, including itself (Engineering 2006). Thus, a satisfactory shielding material must accommodate both incoming and outgoing EMI. It is known that three mechanisms can be invoked for acceptable EMI SE: reflection on the surface of substrate (SE_R), the absorption of electromagnetic energy (SE_A), and multiple-reflection (SE_M) of electromagnetic radiation (Chung 2000). In a homogeneous conductive material, reflection is often the predominant shielding mechanism in which the material deploys mobile charge carriers (holes or electrons) to destructively interfere with incident EM waves. Absorption is a secondary shielding mechanism related to material thickness. The last shielding reason is multiple-reflection considered as interior reflections within shielding materials. EMI SE can be calculated by the following equation (Li et al. 2006; Wang et al. 2008):

$$SE_{total} = 10\log(P_i/P_0) = SE_R + SE_A + SE_M \quad (1)$$

In which the incident P_i is separated by the remaining power (P_0), the reflected power (P_r), and the absorbed power at the shielding output (Thomassin et al. 2007).

In this study, the three dimensional structure of BC may provide a platform for multiple reflection mechanisms to interfere with EMI SE. The EMI mechanisms involved within BC/Cu nanocomposites were investigated by magnetron sputtering (Fig. 1). This study therefore focused on measuring the effect of reflection and multiple-reflection on EMI SE by analyzing appropriate power data. A comprehensive investigation into nanomaterials and their potential application for EMI shielding was conducted.

Experimental section

Materials

Cu target was purchased from Hefei Department of crystal material Technology Co., Ltd (Hefei, China). Non-woven fabric (an area mass of 500 g/m^2) was obtained from Jiangsu Sophie filter material Co., Ltd (Yancheng, China). Woven fabric was purchased from Jiangsu Sinocot International Trade Co., Ltd (Changzhou, China). BC was supplied from in-house lab (Jiangnan university, China). All of the chemicals were of analytical grade and solutions were prepared with distilled water.

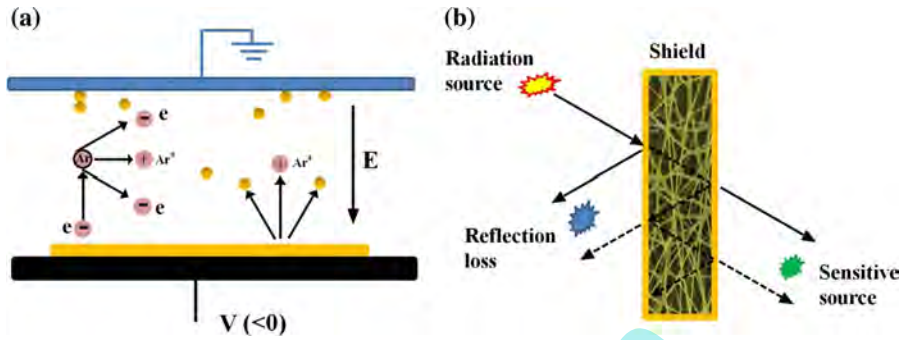

Fig. 1 Schematic representation of the mechanism of: **a** magnetron sputtering; **b** difference between reflection and multiple-reflection (not to scale)

Preparation of BC

BC pellicles were produced by *A. xylinum* (*G. xylinus*) bacterial strain in Hestrin and Schramm (HS) medium (0.6 % glucose, 0.8 % bacto-peptone, 2.5 % yeast) (Toyosaki et al. 1995), which was dissolved in distilled water (neutral pH). The flasks were incubated statically at 30 °C for 7 days. The synthesized cellulose were dipped into 0.1 M NaOH for 4 h at 80 °C to clear the cells and culture liquid (Long et al. 2014). Afterwards, the pretreated BC was rinsed 3 times at pH 7 distilled water.

BC culture process

The growth of *Gxylinus* was conducted over a static culture 6-day track in which it was first added to a 100 ml Erlenmeyer flask containing 10 ml of HS medium (Seok Ho et al. 2006). On day one, the culture solution was a completely transparent orange-colored liquid (Fig. 2a) that became more turbid over time (Park et al. 2009). On the six, the culture began to display membranes (not unlike the original culture color) indicating the gradual formation of a BC pellicle. The sixth day presented gel-like white BC membrane-like structure (Zhou et al. 2013) as shown in Fig. 2a. Figure 2b displays a schematic diagram for the BC formation. Initially, free bacteria adhered to surface bubbles which noticeably presented BC fibers (Czaja et al. 2004). Subsequently, the BC began to form a far more tight structure as single cellulose stands interlinked and progressively accumulated in the static culture solution. With the passage of more time, the rate of BC-formation became slow because of reduced oxygen. The formation of new BC fibrils on existing pellicle was continuous until more uniform, compact, and overlapped fibrils were generated (Nandgaonkar et al. 2014).

Sputter coating

Sputter coating of Cu were conducted on the BC nanofiber surface in a magnetron sputter (JZCK-420B, Juzhi Co., Ltd., China). A Cu target (purity: 99.99 %) was mounted on the cathode. The target was placed below the substrate at a distance of 80 mm and the Cu particles were sputtered on BC film facing the target with rotating speed of 90 rpm to achieve uniform deposition. Water-cooling was applied to control the temperature of the substrate during sputtering, which avoided substrate deformation and the diffusion movement of the sputtered Cu nanoparticles by high temperature. Initially, The chamber was pumped to a pressure of 7.9×10^{-4} Pa before introduction of sputtering Ar gas (purity: 99.99 %). The flow of Ar was set to 21 sccm. During sputtering, three different sputtering powers (30, 50 and 70 W) was set at 0.8 Pa. Coating time was 0, 5, 10, 20, 30, 40 and 50 min, respectively. A schematic preparation method of BC/Cu nanocomposites is shown in Fig. 3. For comparison, the substrate was prepared by similar method except that BC was replaced by non-woven, woven and knitted fabrics.

Measurement and characterization

The surface of pure BC nanofibers was analyzed by FTIR (Nicolet Nexus, Thermo Electron Corporation, Waltham, MA, USA) in the range 4000–400 cm^{-1}. The surface morphologies of the BC nanofibers and BC/Cu nanocomposites were examined by AFM (CSPM 4000, Benyuan, China). All samples were scanned in tapping mode at room temperature in

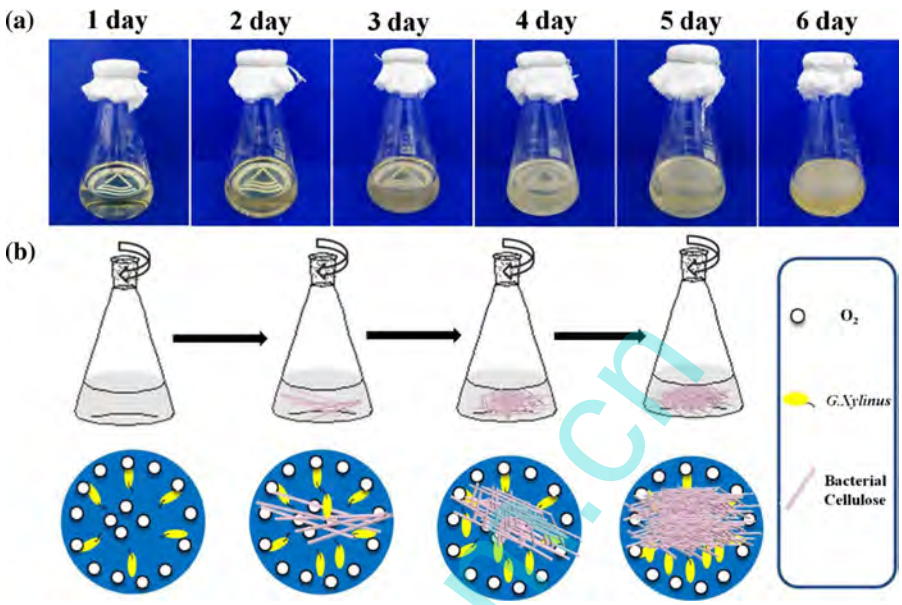

Fig. 2 The cultivation process of BC in the presence of *G. xylinus*: **a** photographic images of 6-day track of BC growth under static conditions; **b** schematic plot of 3D wet web-like BC formation

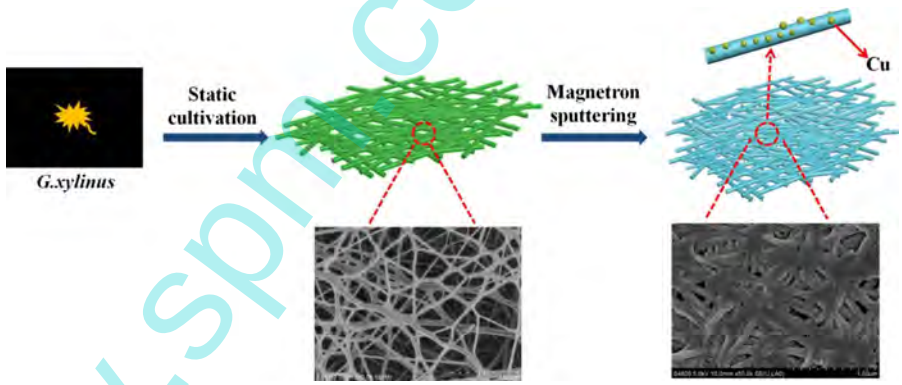

Fig. 3 A schematic preparation method of BC/Cu nanocomposites

atmosphere. Powder D8 Advance X-ray diffraction (XRD, Bruker AXS D8, Germany) and Energy dispersive X-ray spectroscopy (EDX, EDAX-TSL, AMETEK USA) analyzed BC/Cu nanocomposites chemical composition. The thermal stability of the BC/Cu nanocomposites was done using thermal gravimetric analysis (TGA, TGA/1100SF; Mettler Toledo International Trading Co., Ltd. Shanghai, China) at heating rate of 10 °C/min from 25 to 800 °C under N_2. Mechanical properties of the pure BC and BC/Cu materials, whose thickness were measured on a Coating Thickness Meter (Dualscope MPO), were tested using a uniaxial testing machine (INSTRON1185, Instron Corporation, USA) at a tensile rate of 10 mm/min with a clamp distance of 2 cm. An average value was calculated by ten reduplicative tests of each sample of 5 cm in length, 1 cm in width. Conductivity measurements were conducted by a four-point probe (Baishen Technology, China), suitable for testing square resistance and electrical resistivity. All samples were measured ten times in the same direction and averaged. The EMI SE was characterized by using a vector network analyzer (VNA) (Dongnan Univerisity 8573ES, China) using the method of flange coaxial for testing. The range and precision of measuring system is from 0 to 1500 MHz. ASTM-D4935-99 Standard Test Method for Measuring the EMI SE of Planar Materials is shown in Fig. 4.

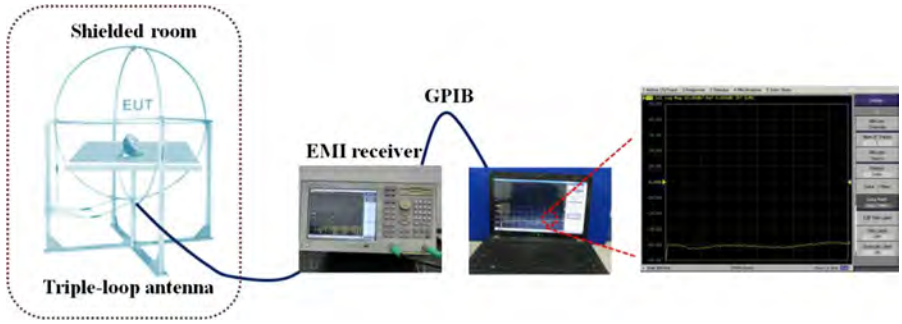

Fig. 4 The schematic plot of EMI SE measurements by a vector network analyzer

Result and discussion

FT-IR

Figure 5 reveals FTIR spectra of pure BC nanofibers. The FTIR spectrum of BC has a band at ~3466 cm^{-1} that can be assigned to stretching of hydrogen bond in –OH (Zhu et al. 2015). The absorption at 2965 cm^{-1} is related to C–H stretching vibrations, consistent with the characteristic bands of BC reported (Barud et al. 2015). The bands at 1163 cm^{-1} were attributed to the C1–O–C4 glycosidic link, while the bands at 1100, 1060 and 1035 cm^{-1} are also assigned to vibrations of C2–O2, C3–O3 and C6–O6 as reported (Kačuráková et al. 2002).

Morphology analyses

AFM images of BC nanofibers before and after the distribution of Cu nanoparticles on the nanofiber surfaces were obtained (Fig. 6a, b). They clearly showed that BC nanofibers have a reticular three-dimensional structure, are ultrafine, and are formed of fiber ranging from nanometer to micron diameters with lengths up to 100 microns. The diameter of the fibrils range from 10 to 70 nm with an average diameter ~40 nm (Haigler et al. 1982; Klemm et al. 2001) (Fig. 6c). After depositing the Cu nanoparticles by magnetron sputtering, the AFM images showed that the BC surface was covered with nanoscale-thick Cu nanoparticles layers. As coating time increased, the Cu nanoparticles coalesced and appeared more uniform; the average size of a cluster was ~70 nm that formed a compact and uninterrupted coating as illustrated in Fig. 6d, e. In Fig. 6f, the average size of the sputtered Cu cluster was ~70 nm, which deviated from the theoretical value described by the Debeye–Scherrer equation (Fig. 8b) largely because of the collisions due to the coated Cu nanoparticle layers. Over time, a more compact deposition was achieved (Xu et al. 2010), as revealed in Fig. 6c.

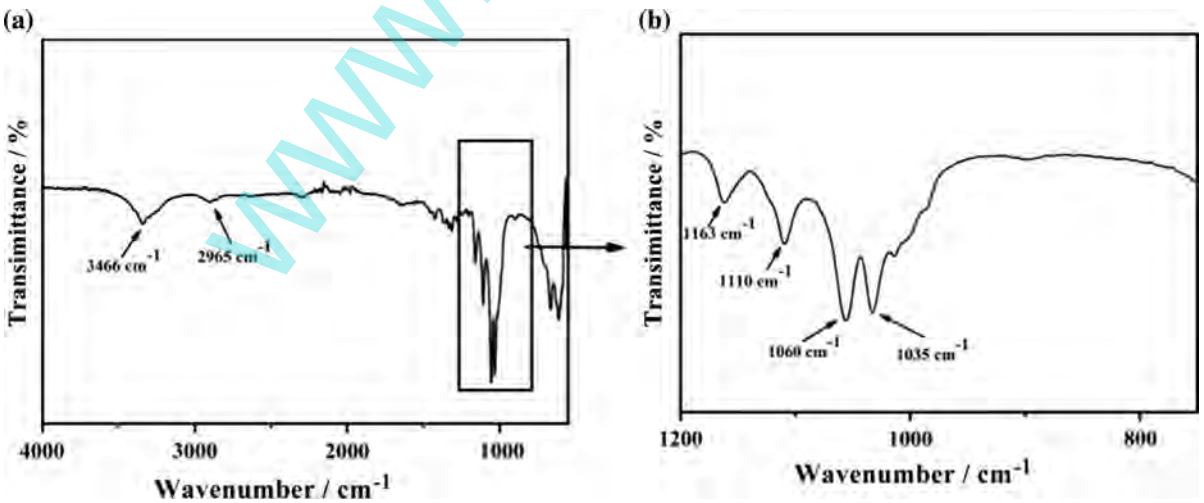

Fig. 5 FTIR spectrograms obtained from pure BC over **a** 4000–500 cm^{-1} and **b** 1200–500 cm^{-1}

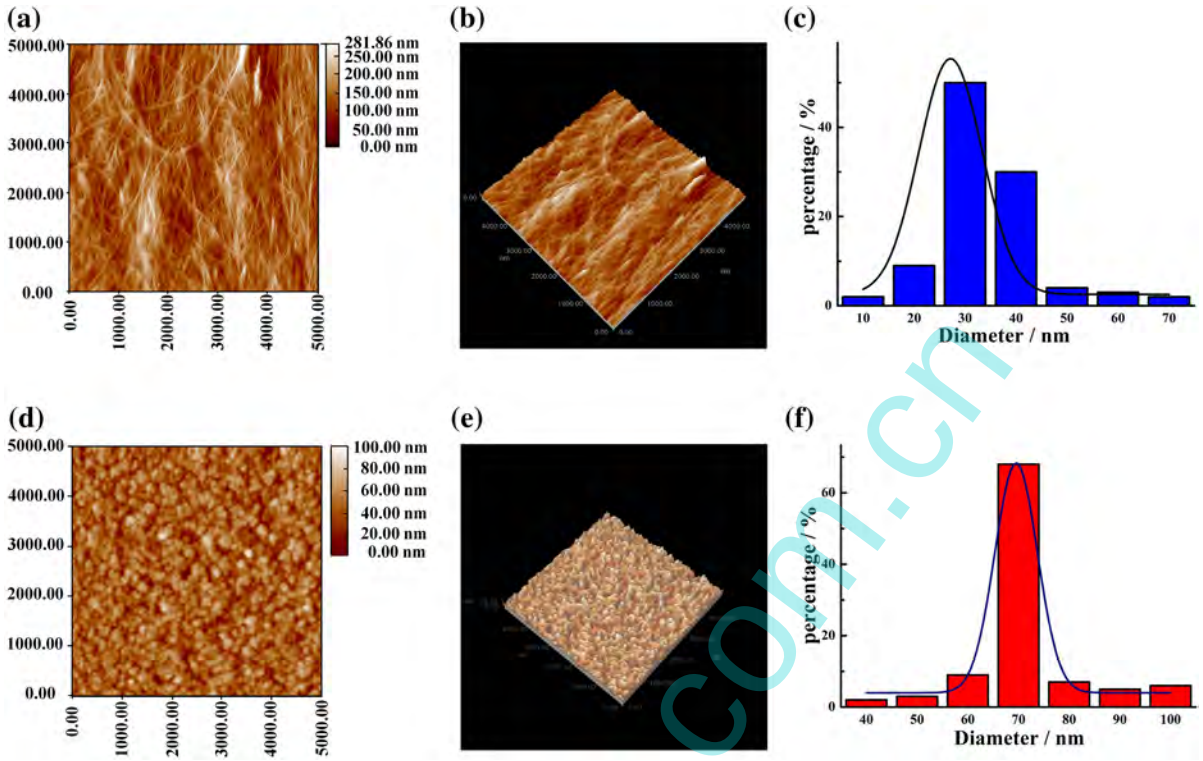

Fig. 6 AFM surface morphologies of **a**, **b** a film of pure BC; **c** diameter distribution of BC nanofibers; **d**, **e** a composite film of BC/Cu; **f** size distribution of Cu nanoparticles

TGA analysis

The thermal stability and thermal decomposition of the BC and BC/Cu nanocomposites film were investigated using TGA (Fig. 7). Two significant weight loss stages were observed from ambient →237 and 237 → 542 °C. The first significant weight loss may be attributed to evaporation of water, whereas the second one at ∼237 °C corresponded to degradation of the main cellulose skeleton (Li et al. 2010). The BC/Cu nanocomposites sample showed three distinct weight losses: the first one occurred over ambient →267 °C, ascribed to physically absorbed and hydrogen bonded linked water molecules (Wang et al. 2010); the second loss from 267 → 361 °C, related to BC dehydration, is ascribed to dehydroxylation and pyrolysis (Gao et al. 2012); the last weight loss terminated at ∼750 °C, where the remaining products are likely copper oxide as revealed in Fig. 7b. This results indicated that the sputtered Cu nanoparticle on the BC nanofibrous substrate enhanced BC thermal stability by a buffer for thermal shock to cellulose chains (Valiokas et al. 2006).

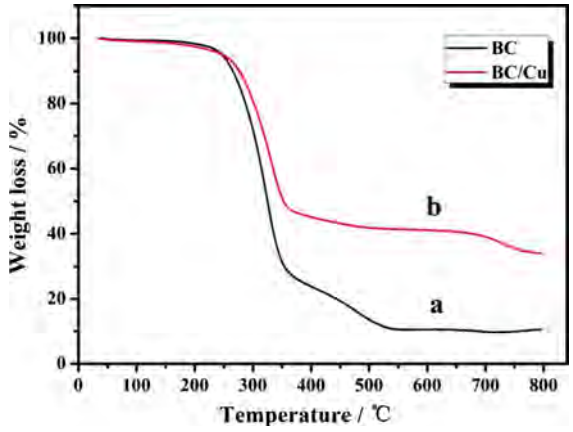

Fig. 7 TGA curve of **a** freeze-dryed BC nanofibers and **b** BC/Cu nanocomposites

EDX and XRD analysis

EDX was used to determine the existence of Cu in the BC/Cu nanocomposites. In Fig. 8a, there were several absorption peaks of Cu in the EDX spectra implying the existence of Cu. XRD was used to further study BC/Cu whose results are displayed in Fig. 8b. The diffraction peaks at ~43.4° corresponded to the (220) plane reflections of copper (Huang et al. 2014). Additionally, the crystallographic planes marked as (100), (010) and (110) corresponded to diffraction angles of 14.6°, 17.6° and 22.6° (French 2014; Ruka et al. 2012; Xiang et al. 2016). The XRD data is shown in Fig. 8b, in which according to the Debeye–Scherrer equation (Jenkins et al. 1996),

$$D = \frac{\kappa\lambda}{\beta \cos\theta} \tag{2}$$

K is shape factor, adopting a typical value of ~0.89, β is the breadth of the observed diffraction line at its half intensity maximum (FWHM), λ is the wavelength of X-ray source used in XRD, and θ corresponds to the peak position (in the current study, $2\theta = 43.4$ for the Cu nanoparticle). The average crystallite size of the Cu nanoparticles was ~14.2 nm. EDS and XRD characterizations jointly demonstrated that the Cu nanoparticles were successfully deposited on BC nanofibers after magnetron sputtering.

Mechanical properties

Mechanical properties were evaluated by tensile strength (TS) and elongation at break (EB). TS is an index of nanofiber strength, whereas EB is an index of nanofibers stretchability before rupture. Figure 9 shows a representative stress–strain curve under uniaxial tensile loading for BC and BC-composite pellicles after 5, 10, 30, and 50 min sputtering. The value of TS of the pure BC was consistent with earlier studies: 20–30 MPa (Mckenna et al. 2009). The addition of BC with different contents of Cu nanoparticles had variable effects on the tensile strength and elongation at break. From the TS (Fig. 9), TS increased for the BC/Cu composites except at 5 min sputtering time, likely due to damage of the surface of BC substrate from unbuffered (no initial layer) sputtering. By comparison with pure BC, the maximum TS value for BC/Cu nocomposites was

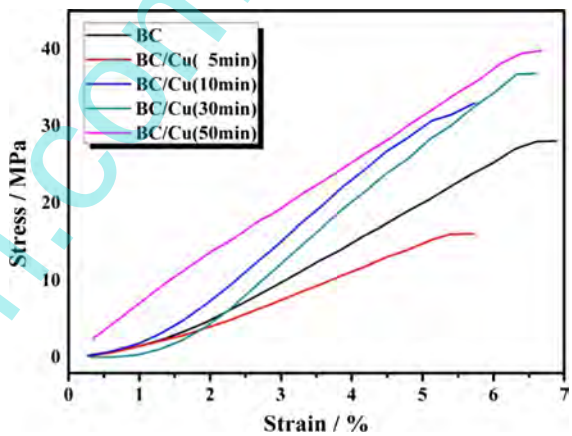

Fig. 9 Tensile stress–strain curves of Cu deposited on BC at different times: 0, 5, 10, 30 and 50 min

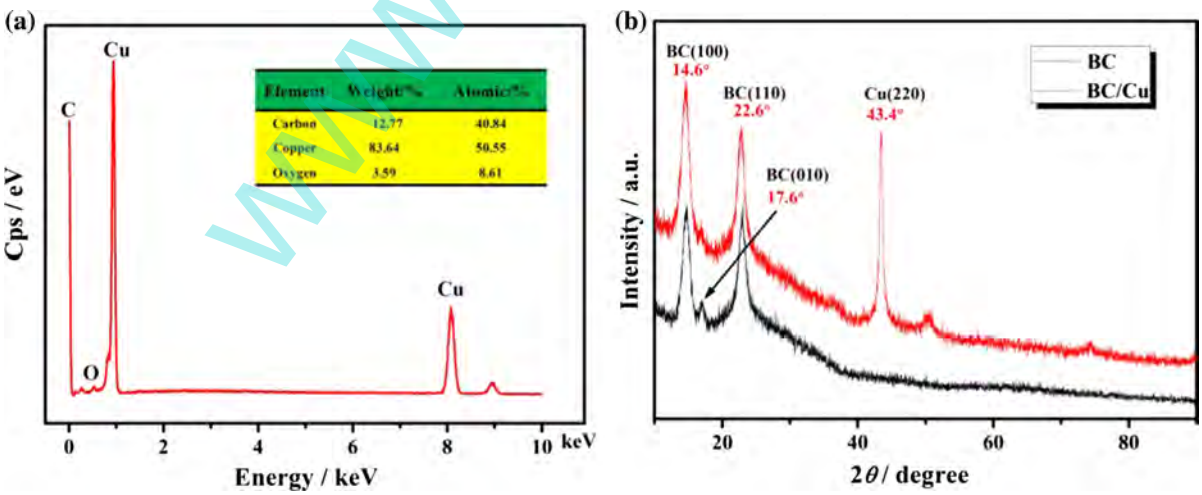

Fig. 8 **a** EDX image of BC/Cu nanocomposites and **b** XRD patterns of pure BC and BC/Cu composites from magnetron sputtering

Table 1 Breaking stress, strain and Young's modulus of Cu deposited on BC at different time

Time (min)	Breaking stress (MPa)	Breaking strain (%)	Young's modulus (MPa)
0	28.11 ± 2.04	6.89 ± 0.27	4.25 ± 0.23
5	16.09 ± 1.87	5.73 ± 0.35	3.51 ± 0.24
10	33.06 ± 2.31	5.74 ± 0.22	6.77 ± 0.35
30	36.87 ± 2.71	6.60 ± 0.37	7.02 ± 0.31
50	41.37 ± 2.95	6.68 ± 0.46	5.86 ± 0.27

~41.4 MPa (Fig. 9). In general, the nanocomposites possessed acceptable mechanical properties for potential EMI materials applications.

The average value and standard deviation of breaking stress, breaking strain and Young's modulus as coating time are shown in Table 1. Firstly, breaking stress, strain and Young's modulus decreased during deposition time (0–5 min). Then, breaking stress, strain and the Young's modulus breaking increased with the increase of coating time (5–30 min). Finally, breaking stress and breaking strain increased, and Young's modulus decreased within coating time (30–50 min). The effect of different time on the BC/Cu composite was investigated. The result indicated that the maximum breaking stress, strain and Young's modulus were 41.37 MPa, 6.68 % and 7.02 MPa, respectively.

Effect of different sputtering conditions on electronic and EMI shielding properties

Electrical conductivity is pivotal for acceptable EMI SE because it can interfere with electromagnetic radiation (Zhang et al. 2011). To study the influence of time on electrical conductivity under different powers, electrical conductivity measurements were done by the four-point probes (Fig. 10a). The electrical conductivity increased with sputtering time for the BC/Cu nanocomposites due to the increase in the deposited Cu layer (Wei et al. 2010). As time increased, copper attached to the BC substrate formed a smoother surface in which the electrical conductivity of the BC/Cu nanocomposites was stable. At 50 min, the nanocomposite at 50 W possessed a relatively higher electrical conductivity (0.026 S m^{-1}) than at 30 and 70 W likely because the copper coating was loose at relatively lower power and the conductivity of BC/Cu nanocomposites may be affected by surface roughness caused at relatively higher power.

Table 2 reveals the relation between and among the thickness, electrical conductivity and shielding effectiveness of the BC/Cu membrane. As the thickness increased, the electrical conductivity and shielding effectiveness increased. When deposition time reached 50 min, BC/Cu nanomaterials displayed high conductivity and acceptable shielding effectiveness.

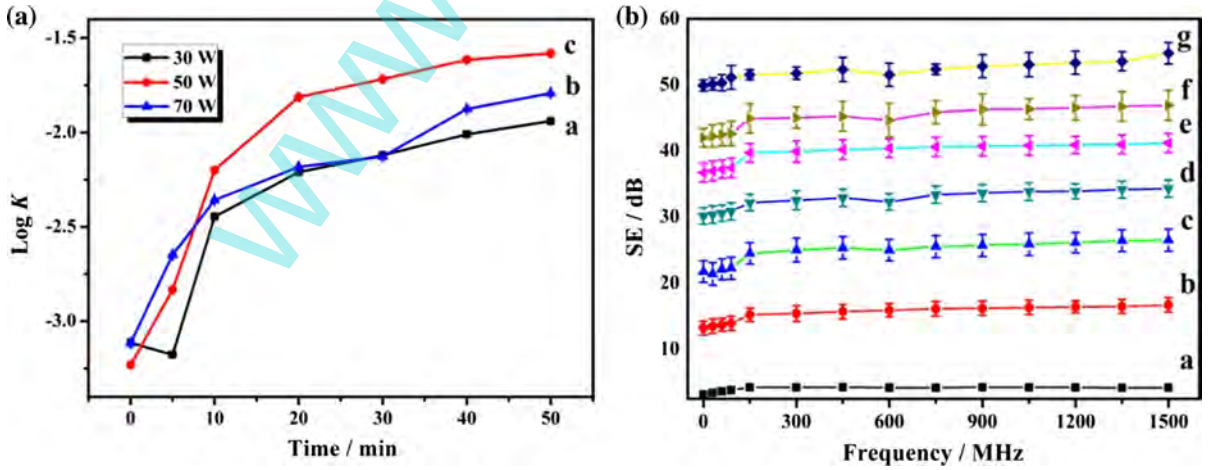

Fig. 10 The effect of **a** time on conductivity of BC/Cu nanocomposite at different powers: *a* 30; *b* 50; *c* 70 W (K is electrical conductivity) and **b** SE of BC/Cu nanocomposite at different coating time (min): *a* 0; *b* 5; *c* 10; *d* 20; *e* 30; *f* 40; *g* 50

Table 2 The relation between and among the thickness, electrical conductivity and shielding effectiveness of the BC/Cu membrane under different deposition time (50 W, 1500 MHz)

Time (min)	Thickness (mm)	Electrical conductivity (S m^{-1})	Shielding effectiveness (dB)
0	$0.232 \pm 4.13 \times 10^{-3}$	∞	4.21 ± 0.40
5	$0.253 \pm 2.64 \times 10^{-3}$	$1.47 \times 10^{-3} \pm 6.27 \times 10^{-5}$	16.70 ± 1.07
10	$0.274 \pm 1.71 \times 10^{-3}$	$6.32 \times 10^{-3} \pm 4.73 \times 10^{-5}$	26.51 ± 1.67
20	$0.323 \pm 1.32 \times 10^{-3}$	$1.54 \times 10^{-2} \pm 6.12 \times 10^{-4}$	34.31 ± 1.30
30	$0.374 \pm 1.17 \times 10^{-3}$	$1.92 \times 10^{-2} \pm 6.02 \times 10^{-4}$	41.20 ± 1.46
40	$0.423 \pm 1.08 \times 10^{-3}$	$2.43 \times 10^{-2} \pm 5.86 \times 10^{-4}$	46.91 ± 2.26
50	$0.462 \pm 1.01 \times 10^{-3}$	$2.63 \times 10^{-2} \pm 5.70 \times 10^{-4}$	55.00 ± 2.98

Table 3 Electrical performance comparison of different substrates coated by copper

Substrates	Electrical conductivity (S m^{-1})	Square resistance (Ω/□)	Shielding effectiveness (dB)	References
Non-woven	$0.116 \pm 8.7 \times 10^{-3}$	0.42 ± 0.09	34.71 ± 1.44	(Meng et al. 2014)
Woven fabric	$0.012 \pm 4.7 \times 10^{-4}$	6.25 ± 0.92	22.63 ± 0.98	
Knitted fabric	$\propto 0$	∞	1.54 ± 0.18	
Bacterial cellulose	$0.026 \pm 5.7 \times 10^{-4}$	2.08 ± 0.12	55.00 ± 2.98	This work

The variation of reflection coefficient of BC/Cu nanocomposites at different coating time and frequencies is given in Fig. 10b. In Fig. 10b, the EMI SE of BC/Cu nanocomposites showed a significant increase with coating time. Two main mechanisms are likely involved in EMI SE: the first shielding mechanism is attributed to Cu particles that are on BC substrate formed a continuous compact structure as time increased so that the absolute values of absorption and reflection increase with a decrease in the square resistance value; the second shielding mechanism may be ascribed to internal reflections within BC substrate in which the efficiency of multiple-reflection was improved by high specific surface area and porous three-dimensional network structure (Dai et al. 2012). In general, the EMI SE of the BC/Cu nanocomposites was enhanced with an increase in film thickness, in which the maximum EMI SE value was 55 dB at 1500 MHz. EMI shielding efficiency included SE_R, SE_A and SE_M, which can be described by $SE_R = 20\text{-}lg|1 + n|^2/4|n|$ and $SE_A = 8.686\alpha l$ (Joo and Epstein 1994), respectively. The SE_R and SE_A ($l = 0.52$ mm) were calculated by using electromagnetic parameters. It was found that total EMI SE arose mainly from reflection at the low frequency range and the absorption in the high range. SE_T was $\sim$55 dB, a value sufficient to meet commercial application SE demands.

Table 3 compares the EMI shielding performance of different substrates. The materials displayed satisfactory results at relatively higher electrical conductivities, had lower square resistances, and excellent EMI shielding properties.

Conclusions

EMI shielding-based BC/Cu nanocomposites were successful prepared by magnetron sputtering of Cu on BC substrates. The Cu nanoparticles were evenly deposited on the surfaces of BC nanofibers to ensure successful realization of the final materials properties. The effect of different conditions on the EMI SE of the BC/Cu composite was investigated to show that the optimum time and power were 50 min and 50 W for the best materials properties. The as-prepared BC/Cu nanoscale materials thus displayed high conductivity, mechanical properties, and acceptable EMI shielding. Additionally, shielding by reflection was found to be dependent on time and power of sputtering. These novel nanocomposites therefore appear to be a promising candidate material for practical applications of EMI shielding.

Acknowledgments This research was financially supported by the Priority Academic Program Development of Jiangsu

Higher Education Institutions, the Natural Science Fundation of Jiangsu Province (BK20150155), Six talent peaks project in Jiangsu Province (2014-XCL001), the Fundamental Research Funds for the Central Universities (JUSRP51505), the Fundamental Research Funds for the Central Universities (JUSRP115A04), and the Fundamental Research Funds for the Central Universities (JUSRP51621A). the Department of Education in Anhui Province of China (2015LJRCTD001), the China Postdoctoral Science Foundation (2014M560391), the China Postdoctoral Science Foundation (2015T80496).

References

Barud HGO, Barud HDS, Cavicchioli M, Amaral TSD, Junior OBDO, Santos DM, Celes F, Borges VM, Oliveira CID (2015) Preparation and characterization of a bacterial cellulose/silk fibroin sponge scaffold for tissue regeneration. Carbohydr Polym 128:41–51

Cao MS, Song WL, Hou ZL, Wen B, Yuan J (2010) The effects of temperature and frequency on the dielectric properties, electromagnetic interference shielding and microwave-absorption of short carbon fiber/silica composites. Carbon 48:788–796

Che RC, Peng LM, Duan XF, Chen Q, Liang XL (2004) Microwave absorption enhancement and complex permittivity and permeability of Fe encapsulated within carbon nanotubes. Adv Mater 16:401–405

Chen S, Zhou B, Hu W, Wen Z, Na Y, Wang H (2013) Polyol mediated synthesis of ZnO nanoparticles templated by bacterial cellulose. Carbohydr Polym 92:1953–1959

Chung DDL (2000) Materials for electromagnetic interference shielding. J Mater Eng Perform 9:350–354

Czaja W, Romanovicz D, Brown RM (2004) Structural investigations of microbial cellulose produced in stationary and agitated culture. Cellulose 11:403–411

Dai B, Shao X, Ren Y, Wang G, Pei C, Ma Y (2012) Electromagnetic performances of composites with promising carbons derived from bacterial cellulose. Mater Lett 82:188–190

Edelstein D, Heidenreich J, Goldblatt R, Cote W, Uzoh C, Lustig N, Roper P, Mcdevitt T, Motsiff W, Simon A (1997) Full copper wiring in a sub-0.25 μm CMOS ULSI technology. In: Proceedings of Iedm

French AD (2014) Idealized powder diffraction patterns for cellulose polymorphs. Cellulose 21:885–896

Gao S, Wang J, Jin Z (2012) Preparation of cellulose films from solution of bacterial cellulose in NMMO. Carbohydr Polym 87:1020–1025

Haigler CH, White AR, Brown RM, Cooper KM (1982) Alteration of in vivo cellulose ribbon assembly by carboxymethylcellulose and other cellulose derivatives. J Cell Biol 94:64–69

Han J, Li Q, Tang L, Chen S, Wang H (2015) Preparation and properties of electromagnetic functional composite membrane based on bacterial cellulose. J Funct Mater 46(14):14083–14087

Huang JC (2003) EMI shielding plastics: a review. Adv Polym Technol 14:137–150

Huang Y, Hang T, Hu A, Chen Z, Lu Q, Li M (2014) Solid state diffusion between Sn and Cu microcones on Cu microcones. J Alloys Compd 582:408–413

Jenkins R, Snyder RL (1996) Introduction to X-ray powder diffractometry. Wiley, London

Jonas R, Farah LF (1998) Production and application of microbial cellulose. Polym Degrad Stab 59:101–106

Joo J, Epstein AJ (1994) Electromagnetic radiation shielding by intrinsically conducting polymers. Appl Phys Lett 65:2278–2280

Kačuráková M, Smith AC, Gidley MJ, Wilson RH (2002) Molecular interactions in bacterial cellulose composites studied by 1D FT-IR and dynamic 2D FT-IR spectroscopy. Carbohydr Res 337:1145–1153

Klemm D, Schumann D, Udhardt U, Marsch S (2001) Bacterial synthesized cellulose-artificial blood vessels for microsurgery. Prog Polym Sci 26:1561–1603

Lakshmi K, John H, Mathew KT, Joseph R, George KE (2009) Microwave absorption, reflection and EMI shielding of PU-PANI composite. Acta Mater 57:371–375

Li N, Huang Y, Du F, He X, Lin X, Gao H, Ma Y, Li F, Chen Y, Eklund PC (2006) Electromagnetic interference (EMI) shielding of single-walled carbon nanotube epoxy composites. Nano Lett 6:1141–1145

Li SM, Jia N, Zhu JF, Ma MG, Sun RC (2010) Synthesis of cellulose–calcium silicate nanocomposites in ethanol/water mixed solvents and their characterization. Carbohydr Polym 80:270–275

Lian T, Han J, Jiang Z, Chen S, Wang H (2015) Flexible conductive polypyrrole nanocomposite membranes based on bacterial cellulose with amphiphobicity. Carbohydr Polym 117:230–235

Liang HW, Guan QF, Zhu Z, Song LT, Yao HB, Lei X, Yu SH (2012) Highly conductive and stretchable conductors fabricated from bacterial cellulose. NPG Asia Mater 4:e19

Long C, Qi D, Wei T, Yan J, Jiang L, Fan Z (2014) Nitrogen-doped carbon networks for high energy density supercapacitors derived from polyaniline coated bacterial cellulose. Adv Funct Mater 24:3953–3961

Marins JA, Soares BG, Barud HS, Ribeiro SJL (2013) Flexible magnetic membranes based on bacterial cellulose and its evaluation as electromagnetic interference shielding material. Mater Sci Eng C 33:3994–4001

Marins JA, Soares BG, Fraga M, Müller D, Barra GMO (2014) Self-supported bacterial cellulose polyaniline conducting membrane as electromagnetic interference shielding material: effect of the oxidizing agent. Cellulose 21:1409–1418

Markham D (1999) Shielding: quantifying the shielding requirements for portable electronic design and providing new solutions by using a combination of materials and design. Mater Des 21:45–50

Mckenna BA, Mikkelsen D, Wehr JB, Gidley MJ, Menzies NW (2009) Mechanical and structural properties of native and alkali-treated bacterial cellulose produced by Gluconacetobacter xylinus strain ATCC 53524. Cellulose 16:1047–1055

Meng LL, Wei QF, Li YL, Xu WZ (2014) Effects of plasma pretreatment on surface properties of fabric sputtered with copper. Int J Cloth Sci Technol 26:96–104

Nandgaonkar AG, Wang Q, Fu K, Krause WE, Wei Q, Gorga R, Lucia LA (2014) A one-pot biosynthesis of reduced graphene oxide (RGO)/bacterial cellulose (BC) nanocomposites. Green Chem 16:3195–3201

Park WI, Kim HS, Kwon SM, Hong YH, Jin HJ (2009) Synthesis of bacterial celluloses in multiwalled carbon nanotube-dispersed medium. Carbohydr Polym 77:457–463

PengFei L, Quan F, QingQing W, GuoHui L, DaWei L, Qufu W (2016) Biosynthesis of bacterial cellulose/carboxylic multi-walled carbon nanotubes for enzymatic biofuel cell application. Materials 9(3):183. doi:10.3390/ma9030183

Petersen N, Gatenholm P (2011) Bacterial cellulose-based materials and medical devices: current state and perspectives. Appl Microbiol Biotechnol 91:1277–1286

Ruka DR, Simon GP, Dean KM (2012) Altering the growth conditions of Gluconacetobacter xylinus to maximize the yield of bacterial cellulose. Carbohydr Polym 89:613–622

Sen B, Hamelin J, Bru-Adan V, Godon J-J, Chandra TS (2008) Structural divergence of bacterial communities from functionally similar laboratory-scale vermicomposts assessed by PCR-CE-SSCP. J Appl Microbiol 105: 2123–2132

Seok Ho Y, Hyoung-Joon J, Moo-Chang K, Ryang PY (2006) Electrically conductive bacterial cellulose by incorporation of carbon nanotubes. Biomacromolecules 7:1280–1284

Song WL, Cao MS, Hou ZL, Fang XY (2009) High dielectric loss and its monotonic dependence of conducting-dominated multiwalled carbon nanotubes/silica nanocomposite on temperature ranging from 373 to 873 K in X-band. Appl Phys Lett 94:233110–233113

Thomassin J, Lou X, Pagnoulle C, Saib A, Bednarz L, Huynen I, Jérôme R, Detrembleur C (2007) Multiwalled carbon nanotube/poly(ε-caprolactone) nanocomposites with exceptional electromagnetic interference shielding properties. J Phys Chem C 111:88–97

Toyosaki H, Naritomi T, Seto AM, Tsuchida T, Yoshinaga F (1995) Screening of bacterial cellulose-producing acetobacter strains suitable for agitated culture. Biosci Biotechnol Biochem 59:1498–1502

Tyagi S, Alavi M, Bigwood R, Bramblett T, Brandenburg J, Chen W, Crew B, Hussein M, Jacob P, Kenyon C (2000) A 130 nm generation logic technology featuring 70 nm transistors, dual Vt transistors and 6 layers of Cu interconnects. In: Electron devices meeting, 2000. IEDM technical digest. International, pp 567–570

Valiokas R, Östblom M, Björefors F, Bo L, Jing S, Konradsson P (2006) Structural and kinetic properties of laterally stabilized, oligo(ethylene glycol)-containing alkylthiolates on gold: a modular approach. Biointerphases 1:22–34

Wang J, Xiang C, Liu Q, Pan Y, Guo J (2008) Ordered mesoporous carbon/fused silica composites. Adv Funct Mater 18:2995–3002

Wang JH, Gao C, Zhang YS, Wan YZ (2010) Preparation and in vitro characterization of BC/PVA hydrogel composite for its potential use as artificial cornea biomaterial. Mater Sci Eng C Mater 30:214–218

Wang B, Li X, Luo B, Yang J, Wang X, Song Q, Chen S, Zhi L (2013a) Pyrolyzed bacterial cellulose: a versatile support for lithium ion battery anode materials. Small 9:2399–2404

Wang M, Anoshkin IV, Nasibulin AG, Korhonen JT, Jani S, Jaakko P, Kauppinen EI, Ras RHA, Olli I (2013b) Modifying native nanocellulose aerogels with carbon nanotubes for mechanoresponsive conductivity and pressure sensing. Adv Mater 25:2428–2432

Wei Q, Shao D, Deng B, Xu Q (2010) Functionalization of ceramic fibers by metallic sputter coating. J Coat Res 7:99–103

Wen L, Ma Y, Dai B, Zhou Y, Liu J, Pei C (2013) Preparation and dielectric properties of SiC nanowires self-sacrificially templated by carbonated bacterial cellulose. Mater Res Bull 48:687–690

Xiang ZY, Gao WH, Chen LH, Lan W, Zhu JY, Runge T (2016) A comparison of cellulose nanofibrils produced from Cladophora glomerata algae and bleached eucalyptus pulp. Cellulose 23:493–503

Xu Y, Wang H, Wei Q, Liu H, Deng B (2010) Structures and properties of the polyester nonwovens coated with titanium dioxide by reactive sputtering. J Coat Res 7:637–642

Yang S, Lozano K, Lomeli A, Foltz HD, Jones R (2005a) Electromagnetic interference shielding effectiveness of carbon nanofiber/LCP composites. Compos Part A Appl Sci Manuf 36:691–697

Yang Y, Gupta MC, Dudley KL, Lawrence RW (2005b) Novel carbon nanotube-polystyrene foam composites for electromagnetic interference shielding. Nano Lett 5: 2131–2134

Zhang HB, Yan Q, Zheng WG, He Z, Yu ZZ (2011) Tough graphene-polymer microcellular foams for electromagnetic interference shielding. ACS Appl Mater Interfaces 3:918–924

Zheng WL, Hu WL, Chen SY, Zheng Y, Zhou BH, Wang HP (2014) High photocatalytic properties of zinc oxide nanoparticles with amidoximated bacterial cellulose nanofibers as templates. Chin J Polym Sci 32:169–176

Zhou T, Chen D, Jiu J, Nge TT, Sugahara T, Nagao S, Koga H, Nogi M, Suganuma K, Wang X (2013) Electrically conductive bacterial cellulose composite membranes produced by the incorporation of graphite nanoplatelets in pristine bacterial cellulose membranes. Express Polym Lett 7:756–766

Zhu W, Li W, He Y, Duan T (2015) In-situ biopreparation of biocompatible bacterial cellulose/graphene oxide composites pellets. Appl Surf Sci 338:22–26